Lab on a Chip

Accepted Manuscript

This is an *Accepted Manuscript*, which has been through the Royal Society of Chemistry peer review process and has been accepted for publication.

Accepted Manuscripts are published online shortly after acceptance, before technical editing, formatting and proof reading. Using this free service, authors can make their results available to the community, in citable form, before we publish the edited article. We will replace this *Accepted Manuscript* with the edited and formatted *Advance Article* as soon as it is available.

You can find more information about *Accepted Manuscripts* in the **Information for Authors**.
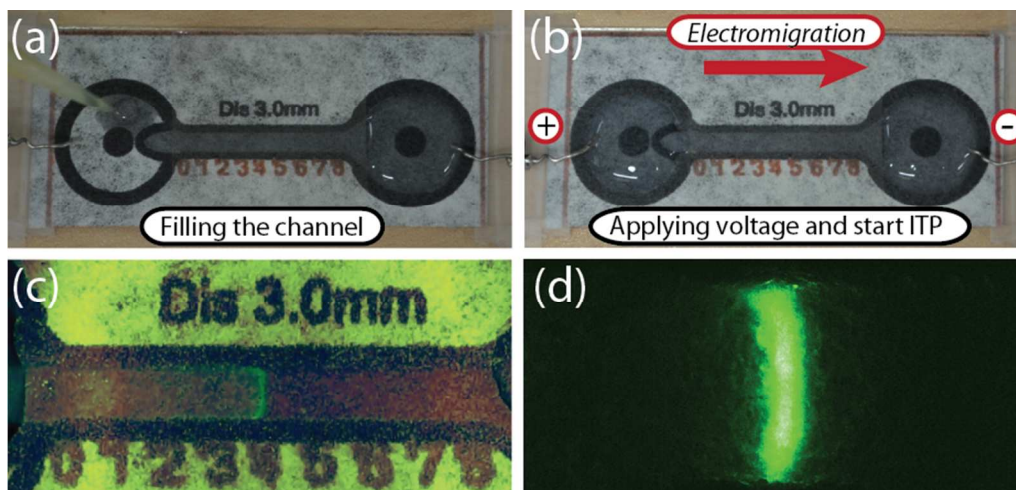
We present a novel paper-based analytical device for isotachophoretic sample focusing, enabling processing of 30 µL and 1,000-fold increase in concentration in several minutes.

1,000-FOLD SAMPLE FOCUSING ON PAPER-BASED MICROFLUIDIC DEVICES

Tally Rosenfeld[1] and Moran Bercovici[1,*]

[1] Faculty of Mechanical Engineering, Technion – Israel Institute of Technology, Haifa 32000, Israel
[*] Corresponding author

Abstract

We present an experimental and analytical study of a novel paper-based analytical device (µPAD) for isotachophoretic sample focusing. Guided by a simple heat transfer model, we further developed wax-printing fabrication to enable the creation of shallow channels which are critical in providing sufficient dissipation of joule heat, and thus enable the use of high electric fields and short analysis time. This results in a device that is self-contained on a simple piece of filter paper and does not require any specialized enclosures or cooling devices to combat evaporation of high temperatures. Furthermore, we provide an analytical model for isotachophoretic sample accumulation in porous media, introduce a simple figure of merit for evaluating and comparing the efficiency of such devices, and present experimental validation in both paper and glass channels. Using this device we demonstrate the processing of 30 µL of sample achieving 1,000-fold increase of peak concentration in 6 min. We believe this method and device can serve to guide the design of low-cost, rapid and highly sensitive paper-based diagnostic platforms.

1. Introduction

Microfluidic paper-based analytical devices (µPADs) have recently gained significant attention, due to their potential as a low cost, durable, multiplexed, and easy-to-use diagnostic platform. µPADs, first introduced by Martinez *et al.*,[1] are formed by patterning paper into hydrophilic regions, bounded by regions of hydrophobic material. A variety of methods, including wax printing, CO_2 laser cutting, and photolithography now exist for fabrication of such devices[2,3], and they have found use in a variety of biochemical applications including glucose monitoring, detection of heavy metals, nanoparticle-based detection, total protein measurements, and ELISA.[2,4–8] However, despite well identified biomarkers, many diagnostic needs cannot be met by the current sensitivity of such assays.[8,9] The application of low-cost and rapid assays, capable of accurately and sensitively detecting disease at the point-of-care, could have a significant impact on global health, enabling access to advanced molecular diagnostics even in under-resourced and rural areas. We here present a method for significantly increasing the sensitivity of such tests by coupling them with isotachophoresis (ITP).

ITP is an electrophoresis technique which allows for simultaneous separation and preconcentration of analytes based on their effective electrophoretic mobility. ITP has its roots in the fundamentals developed by Kohlrausch,[10] over a century ago, and in moving boundary electrophoresis (MBE) developed in the 1920's and 30's.[11–13] Notably, filter paper was used as substrate for electrophoresis as early as 1951,[14] before the introduction of gel electrophoresis[15] or capillary-based electrophoresis.[16] In the 70's and 80's, renewed interest in ITP lead to its first implementations on paper substrates including cellulose acetate membrane (CAM) and filter paper.[17–19] ITP was used to directly focus or separate proteins of interest from urine,[20] as well as to establish electroosmotic flow (EOF) patterns for delivery of target proteins to immunosensing sites. To mitigate excessive joule heating and evaporation, experimental setups either housed the membrane in a closed chamber,[21,22] used external cooling components as part of their

apparatus,[17,21] or used cellogel film which holds a high water content in its gel matrix.[22] In addition, experiments were run at relatively low electric fields, resulting in several hours of analysis time.[20]

Other electrokinetic techniques have been demonstrated on paper substrates. Mandal *et al.*[23] demonstrated electrokinetic control of liquid transport in a paper-based device, and Ge *et al.*[24] were the first to demonstrate electrophoretic separation on μPAD. Recently (in work published during preparation of this manuscript), Moghadam *et al.*[25] demonstrated ITP focusing on a nitrocellulose membrane housed in an acrylic device containing the reservoirs. The authors have addressed the challenge of evaporation by augmenting their main channel with a cross channel which is dipped in solution and provides additional hydration to the membrane. We here present a different approach and introduce a novel μPAD for isotachophoresis focusing, which is self-contained on a simple piece of paper, does not require any specialized enclosures or cooling devices and enables over 1,000-fold focusing of 30 μL of sample in 10 min. Importantly, we overcome joule heating by designing our fabrication process such that a thick layer of wax deposited at the bottom of the channel enables the creation of shallow channels, resulting in sufficiently rapid heat dissipation.

In section 2.1 we present a simple model for the rate of sample accumulation under ITP in porous media, and define convenient figures of merit which allow direct comparison of extraction efficiency between standard microchannels and paper-based devices. We further provide scaling arguments for the generation and dissipation of heat on such devices, which directly guide the fabrication process. In section 3.1, we provide detailed information on the fabrication of shallow channels, and finally in section 4 we characterize the performance of our devices, demonstrating lossless focusing of finite sample injections, and 1,000-fold sample focusing in less than 6 min for infinite sample injections.

2. Theory

2.1. Sample accumulation under ITP in porous media

ITP is an electrophoresis technique that uses a discontinuous buffer system to focus sample ions of interest at a sharp electric field gradient, formed between high electrophoretic mobility leading ions (LE), and low electrophoretic mobility trailing ions (TE). We here focus our discussion on peak-mode ITP, which is characterized by sample concentrations that are significantly lower than those of the background buffers, and thus do not affect the conductivity or the electric field in the channel.[26]

A useful model for porous media used in several applications[27,28] is based on reducing the complex geometry to a network of independent tortuous capillaries (or 'pores') embedded in a solid. Analysis is simplified to consider a single pore and is then extended to the entire area by summation over all pores.
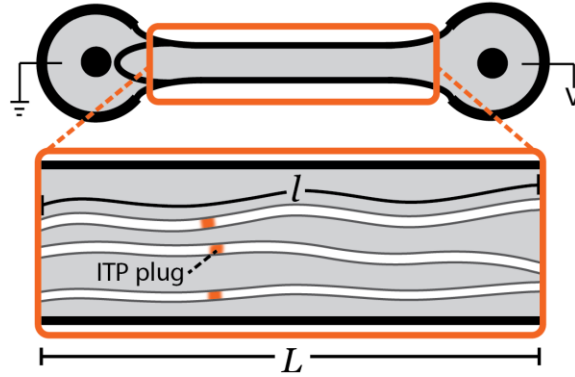
Figure 1. *Schematic illustration of ITP in an idealized porous media, composed of a network of independent tortuous capillaries (or 'pores') embedded in a solid. The average pore length is denoted by l, while the physical length of the porous media (external dimension) is denoted by L. All pores experience the same electric field V, resulting in multiple ITP focusing zones electromigrating simultaneously at a velocity which depends on the tortuosity of each pore. The total void cross-section area (i.e. pore area) is A_e, and the physical cross-section material area is A.*

Assuming an array of n cylindrical pores, the porosity of the porous media, ε, is expressed as the ratio of the void volume of all the pores to the total volume of the substrate[28],

$$\varepsilon = \frac{V_{void}}{V_{total}} = \frac{nA_p l}{AL} \ ,$$

(1)

where A_p is the average pore cross-section area, l is the average pore length, and A and L are respectively the physical cross-section area and length of the porous media (see Fig. 1). The tortuosity is defined as[28]

$$\tau = \left(\frac{l}{L}\right)^2 \ ,$$

(2)

which can then be used to express the effective area of the porous media as a function of measurable parameters

$$A_e = nA_p = \frac{\varepsilon}{\sqrt{\tau}} A \ .$$

(3)

Taking a moving control volume around the ITP interface within a single pore, the rate of analyte ions entering the LE-TE interface is governed by the difference between the analyte ions' velocity in the adjusted TE zone, and the velocity of the ITP interface. The sample accumulation rate in peak-mode ITP within one pore is given by[26]

$$\left.\frac{dN_a}{dt}\right|_{pore} = \left(V_a^{TE} - V_{ITP}\right)c_a^{TE} A_p \ ,$$

(4)

where c_a^{TE} is the concentration of the analyte in the adjusted TE zone. We note that eq.(4) holds irrespectively of electroosmotic flow (EOF) in the system, which equally affects all velocity components.

3

Defining the electrophoretic mobility of species X in zone Y as μ_X^Y, and the electric field in zone Y as E^Y, substituting the ITP condition $V_{ITP} = \mu_L^{LE} E^{LE} = \mu_T^{TE} E^{TE}$, and using the relation $V_a^{TE} = \mu_a^{TE} E^{TE}$, eq.(4) can be expressed as

$$\left.\frac{dN_a}{dt}\right|_{pore} = \left(\frac{\mu_a^{TE}}{\mu_T^{TE}} - 1\right)\mu_L^{LE} E^{LE} c_a^{TE} A_p \; . \tag{5}$$

Summing for all n pores to express the sample accumulation rate in the entire channel, and relating the concentration of the analyte in the TE to that in the reservoir, $c_a^{TE} = \dfrac{\sigma_T^{TE}}{\sigma_T^{well}} c_a^{well}$, we obtain,

$$\frac{dN_a}{dt} = \sum_1^n \left.\frac{dN_a}{dt}\right|_{pore} = \left(\frac{\mu_a^{TE}}{\mu_T^{TE}} - 1\right)\frac{\sigma_T^{TE}}{\sigma_T^{well}} \mu_L^{LE} E^{LE} c_a^{well} \frac{\varepsilon}{\sqrt{\tau}} A \; . \tag{6}$$

where σ_T^{TE} is the TE conductivity in the adjusted TE zone, and σ_T^{well} is the TE conductivity in the TE well. A constant voltage, V, applied across the channel, can be expressed as a function of the electric field in the TE and the LE zones via

$$V = E^{TE} l^{TE} + E^{LE} l^{LE} \; , \tag{7}$$

where l^{TE} and l^{LE} are the (time varying) lengths of the pore segments filled with TE and LE, respectively. Substituting the TE electric field from the current conservation condition, $E^{TE} = \dfrac{\sigma_L^{LE}}{\sigma_T^{TE}} E^{LE}$, the electric field in the LE zone can be expressed as

$$E^{LE} = \frac{V}{\sqrt{\tau} L^{LE}\left(\dfrac{\sigma_L^{LE}}{\sigma_T^{TE}}\dfrac{L^{TE}}{L^{LE}} + 1\right)} \; . \tag{8}$$

Substituting the electric field into eq.(6), we obtain

$$\frac{dN_a}{dt} = \left(\frac{\mu_a^{TE}}{\mu_T^{TE}} - 1\right)\frac{\sigma_T^{TE}}{\sigma_T^{well}}\frac{\mu_L^{LE}}{\sigma_L^{LE}}\left[\frac{\dfrac{\varepsilon}{\tau} A V}{\dfrac{L^{LE}}{\sigma_L^{LE}}\left(\dfrac{\sigma_L^{LE}}{\sigma_T^{TE}}\dfrac{L^{TE}}{L^{LE}} + 1\right)}\right] c_a^{well} \; . \tag{9}$$

Eq.(9) represents the focusing rate at a given voltage, and decreases in time as the ITP interface propagates and L_{TE} increases. As expected, it shows direct dependence on the porosity and tortuosity of the media. However, noting that the expression in brackets is precisely the electric current across the entire channel, I,

$$I(t) = \sum_1^n I_p(t) = \sum_1^n \frac{V}{\left(\dfrac{l^{TE}}{\sigma_T^{TE}} + \dfrac{l^{LE}}{\sigma_L^{LE}}\right)} A_p = \frac{\dfrac{\varepsilon}{\tau} A V}{\dfrac{L^{LE}}{\sigma_L^{LE}}\left(\dfrac{\sigma_L^{LE}}{\sigma_T^{TE}}\dfrac{L^{TE}}{L^{LE}} + 1\right)} \; , \tag{10}$$

allows further simplification of the expression to the form

4

$$N_a(t) = \left(\frac{\mu_a^{TE}}{\mu_T^{TE}} - 1 \right) \frac{\mu_L^{LE}}{\sigma_L^{LE}} \sigma_T^{TE} \int_0^t \frac{c_a^{well}}{\sigma_T^{well}} I(\tau) d\tau \ . \tag{11}$$

Importantly, when expressed as a function of the electric current, I, sample accumulation shows no direct dependence on the cross-section area, nor on porous media parameters. Hence, this expression can be used to describe sample accumulation in both porous and non-porous substrates (e.g. typical glass microchannels). For ideal conditions, where the parameters in the reservoir remain constant in time, and the analyte concentration in the reservoir equals to its initial concentration, c_a^0, we may write

$$N_a(t) = \left(\frac{\mu_a^{TE}}{\mu_T^{TE}} - 1 \right) \frac{\mu_L^{LE}}{\sigma_L^{LE}} \frac{\sigma_T^{TE}}{\sigma_T^{well}} c_a^0 \int_0^t I(\tau) d\tau \ . \tag{12}$$

We thus choose to define

$$\eta = \frac{N_a(t)}{c_a^0 \int_0^t I(\tau) d\tau} \ , \tag{13}$$

as an indicator for the ITP focusing efficiency. η has units of $[lit\, A^{-1} sec^{-1}]$, and reflects the ability of the assay to process a certain sample volume per unit current and time. For constant reservoir conditions, as indicated by eq.(12), the value of η is constant and can be estimated numerically using simulation software such as PeakMaster[29], Simul[30] or Spresso[31]. Such estimations must account though for dependencies on effects such as pH, ionic strength, or temperature. Alternatively, as we show in section 4.2, it can be measured experimentally by monitoring both the amount of accumulated sample and the integral of current. We emphasize that while we expect variations in EOF, channel geometry and topology to be reflected in electric current measurements, for an ideal system with no changes in reservoir conditions, the value of η should, in theory, remain constant for a given system of species, regardless of geometry or substrate material. In section 4.2, we refer again to this ratio for evaluation of the efficiency of our paper-based devices compared to conventional glass microchannels.

Deviations from the ideal model

When implemented in a standard microchannel or microcapillary, the volume of the channel is typically on the order of ~10 nL, significantly lower than the order ~10 µL reservoir, and thus conditions in the reservoir may be assumed constant. However, our paper-based devices are intended for processing a large volume and may hold several µL. As a result, both depletion of sample ions from the TE reservoir and dilution of the TE reservoir by incoming electroosmotic flow (for anionic ITP) may result in a decrease in analyte concentration,

$$c_a^{well}(t) = \frac{c_a^0 V_0 - \int_0^t \frac{dN_a}{dt} dt}{V_0 + \int_0^t u_{EOF} A_e dt} \ , \tag{14}$$

5

where V_0 is the initial volume of the TE reservoir, and u_{EOF} is the area-averaged velocity due to EOF. In addition to these effects, in the absence of convection, the concentration of sample at the entrance to the channel may be diffusion limited, i.e. the diffusion rate of new sample ions to the channel entrance may not be sufficient to compensate for the high flux into the channel. Finally, mobilities and conductivities are a strong function of temperature and their values may be affected by joule heating.

2.2. Joule heating in µPAD

In our initial attempts to perform ITP on paper, we created channels which were based on the entire thickness of the filter paper (approximately 150 µm deep). Such designs exhibited high temperatures leading to rapid evaporation of the liquid and occasionally even autoignition of the paper. Thus, better thermal management of paper-based devices was required for electrokinetic applications. Aiming to maintain a simple and low-cost device, we did not wish to add any external heat-removing devices, and instead studied the potential for a geometrical design that would prevent excessive heating. We here present our model for intra-paper temperature under an applied electric field, whose results guided the fabrication process described in section 3.1.
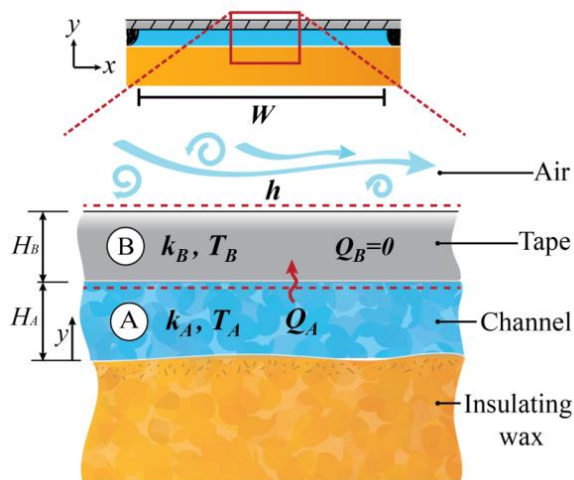
Figure 2. *Schematic representation of the heat transfer problem. Region A represents the paper channel, occupied by the liquid, and region B represents the sealing material (i.e. tape). The bottom wax layer is assumed to be perfectly insulating. Heat is generated in region A, dissipates through the tape and is removed by free convection in air.*

As illustrated in Fig. 2, we consider the cross section of a paper channel sealed from bottom and top by wax and masking tape, respectively. We divide the problem into two different regions; the paper channel is denoted as A, and the sealing material (e.g. masking tape) is marked as B. Moreover, we assume the width of the channel, W (typically on the order of several mm to several cm), is much larger than its depth, H_A (typically in the order 10-100 µm), and therefore the problem can be treated as a 1D problem in the y (depth)-direction. The governing equations for the problem can thus be written as

$$\frac{d^2 T_A}{dy^2} = -\frac{E^2 \sigma}{k_A} \qquad 0 \le y \le H_A,$$

$$\frac{d^2 T_B}{dy^2} = 0 \qquad H_A \le y \le H_A + H_B,$$

(15)

where T_X is the temperature within region X, k_A is the thermal conductivity of the liquid in the channel, $Q_A = E^2 \sigma$ is the heat per unit volume generated during electrophoresis in the channel (region A), E is the electric field, and σ is the conductivity of the buffer. No heat is generated in region B. H_A is depth of the paper-channel containing the liquid, and H_B is the thickness of the masking tape.

The Biot number, $Bi = \frac{hH}{k}$, relates the time scales of heat conduction inside the body and heat convection from its surface, with h denoting the heat transfer coefficient (typically in the range of $2-25\ [W\,m^{-2}K^{-1}]^{32}$ for the free convection of gases), and H representing the characteristic length (here the depth of the channel on the order of 10-100 μm). The thermal conductivity of water, waxes and polymers used in this work are all on the order $k \sim 0.1-1\,[W\,m^{-1}K^{-1}]^{32}$, resulting in a very small Biot number, $Bi \sim 10^{-5}-10^{-1} \ll 1$. This indicates that convection from the surface is significantly slower than conduction within the body, and thus the temperatures within each of the regions, T_A and T_B, can be assumed to be uniform.

Equating the heat fluxes at the interface between region A and B, and at the interface between region B and the air, and using the assumption of $Bi \ll 1$ yields the simple solution

$$\Delta T = T_A - T_\infty = \frac{\sigma E^2 H_A}{h} \ ,$$

(16)

where T_∞ is the temperature far from the device (room temperature). The solution shows that the increase in intra-paper temperature, T_A, is proportional to the square electric field, the conductivity of the electrolyte, and the depth of the channel, and is inversely proportional to the heat transfer coefficient, h. The product σE^2 is highest in the TE region. The conductivity of our buffer is of the order $\sigma \sim 0.1\,[S\,m^{-1}]$, and the electric field is on the order of $E \sim 10^4\,[V\,m^{-1}]$. Assuming a heat transfer coefficient of $10\,[W\,m^{-2}K^{-1}]$, the temperature difference is then given roughly by $\Delta T \sim 10^6 H_A$ (where H_A is in units of meters), i.e. 150 μm thick paper would result in a temperature increase of roughly 150 K.

Clearly, the temperature can be most efficiently reduced by lowering the electric field (by decreasing the voltage used). However, this will also result in a diffused ITP interface and an increase in total analysis time. Lower LE concentration (resulting in lower conductivities) could also be used. However, this would also eliminate TE concentration adaptation which is a source of significant increase in focusing rate. Thus, in order to maintain high electric fields in the system, without excessive joule heating, one should reduce the paper channel depth, H_A, as much as possible. As described in detail in the Experimental section, reducing the thickness of the paper from 150 μm to the range 10-50 μm is sufficient to reduce the temperature to an operational range. Our fabrication process, as described in section 3.1, was specifically designed to achieve this goal.

7

3.   Experimental

3.1. Fabrication of shallow channel μPADs

The method of fabricating μPADs by wax printing,[33,34] has now been widely used owing to its low-cost and simplicity. The technique is based on patterning a hydrophilic paper (or other porous membranes)[35] with hydrophobic wax barriers. Upon heating, the wax melts and penetrates by capillary action through the entire thickness of the paper, and serves as side walls for the paper-channel. We further developed this technique to be compatible with electrokinetic assays. Instead of printing only one layer of wax that wicks through the entire thickness of the paper, we print wax on both sides of the paper. Upon heating, both layers wick into the paper until they meet, resulting in channels that are significantly shallower (~50 μm) than the original thickness of the paper. Such shallow channels are critical in providing sufficient dissipation of joule heat, as detailed in section 2.2, and thus enable the use of high electric fields and short analysis time.

We use cellulose filter paper (125 mm diameter, grade 595, Whatman, GE Healthcare) as our substrate, as it is relatively thin (150 μm thickness) and provides medium-fast flow rate compared to other filter papers. We choose cellulose as our substrate as it does not contain active functional groups and thus is expected to have only weak interaction with biomolecules.[36] We cut the paper to fit A6 paper-size width using a guillotine (3020, KW-trio, Changua, Taiwan). We then design the device's geometry in Autodesk AutoCAD 2013 (Autodesk Inc, San Rafael, CA), and fabricate the microfluidic paper-chip by printing (ColorQube 8570DN, Xerox Corporation, Norwalk, CT) the channel side walls template on one side of the paper, followed by a layer of wax on the opposite side, forming the bottom of the channel. After printing, the two layers are not yet in contact. In order to create a closed channel, we then heat the paper using a temperature-controlled lamination machine (335 R6, SKYDBS Co., Seoul, Korea), which provides uniform heating and can be controlled to provide penetration of the wax to the desired depth.

Different temperatures provide different channel depths. At low temperatures, less than 75°C, the wax penetration level is insufficient, and the side walls created do not reach the bottom layer of wax. This results in leakage from the channel upon filling. At high temperatures, over 105°C, the bottom layer of wax may penetrate the paper entirely and block the channel. We found the optimal lamination temperature, providing shallow yet unblocked channels, to be 95°C, at a feeding speed of 1350 mm/min. We measured the obtained paper channel depth by cutting the paper using a guillotine in a direction perpendicular to the channel, placing the piece between two glass slides for mechanical stability and imaging the cross section area under the microscope (see Fig. 3). At these conditions we estimated the average depth of 50 μm. Finally, in order to prevent evaporation, we cover the channel with a transparent tape (type 8911, 3M, Saint Paul, MN), while both reservoirs are kept open to the atmosphere. The nominal paper channel dimensions used for all experiments are, 2.6 cm length, 2.5 mm width and 50 μm depth. The channel is connected on either end to 6.5 mm radius circular reservoirs. Fig. 3 presents the fabrication process of our paper-based device, and a 3D view image of the device.
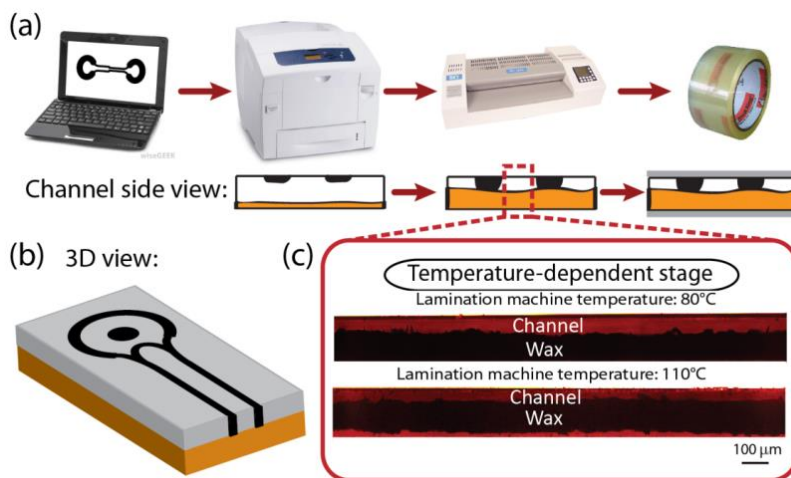
Figure 3. *(a) Schematic illustration of the multistep fabrication process. We print the channel side walls template (black regions) on one side, and a thick wax layer (orange region) on the other side of the paper. The channel is designed to be 2.5 mm wide and is connected to 6.5 mm radius round reservoirs. We then pass the paper through a temperature-controlled laminator which melts the wax and allows it to penetrate to the desired depth. Finally, to prevent evaporation, we cover the channel with a transparent tape, while both reservoirs are kept open to the atmosphere. (b) 3D illustration of the resulting structure. On one end of the channel (TE reservoir) we printed a hydrophobic wax barrier, which stops the flow of the LE, and serves as a repeatable starting point for ITP. (c) Raw fluorescence images of the paper cross-section showing the effect of lamination temperature on the penetration of wax into the paper, resulting in control of the channel depth.*

3.2. Experimental setup

We obtained images using an upright epifluorescent microscope (Eclipse Ci-L, Nikon, Tokyo, Japan) equipped with a 660 nm LED light source (M660L3-C3, Thorlabs Inc., Newton, NJ) and filter-cube (Cy5-4040C-000: 628/40 nm excitation, 692/40 nm emission and 660 nm dichroic mirror, Semrock Inc., Rochester, NY). We used a 1X objective (NA = 0.04, WD = 3.2 mm, Plan UW, Nikon, Tokyo, Japan) for the experiments in paper devices, and a 10X objective (NA = 0.3, WD = 16 mm, Plan Fluor, Nikon, Tokyo, Japan) for the experiments in glass channels. Images were captured using a 14 bit, 1392 x 1040 pixel array CCD camera (Clara DR-2584, Andor, Belfast, Ireland) cooled to -19.5°C. Images of the ITP focusing were taken using an exposure time of 100 ms. When not imaging, the light source was shuttered to prevent photobleaching of the dye. We controlled the camera using NIS Elements software (v.4.11, Nikon, Japan) and processed the images with MATLAB (R2011b, Mathworks, Natick, MA). All ITP experiments were performed at constant voltage, using a high voltage sourcemeter (model 2410, Keithley Instruments, Cleveland, OH).

3.3. Isotachophoresis assay and choice of experiments conditions

In all experiments, we used 100 mM HCl, 200 mM Bistris, and 1% 1.3 MDa poly(vinylpyrrolidone) (PVP) as the LE solution. Our analyte was DyLight650 (NHS Ester, Thermo Fisher Scientific, Waltham, MA) which has its peak fluorescence at an excitation wavelength of 652 nm. We mixed the analyte with the TE solution to get an initial concentration of 10 nM DyLight650 in the reservoir. We used two sets of TE solutions; the first TE set was composed of 100 mM Hepes, 200 mM Bistris, and 1% PVP; the second TE set was composed of 10 mM Tricine, 20 mM Bistris, and 1% PVP. The former set was used for the experiments comparing the focusing efficiency of paper devices to glass channels. The latter set was used for demonstration of maximum focusing in paper. PVP was added to the LE and TE solutions for suppression of electroosmotic flow (EOF). We used high ionic strength LE to maximize the focusing rate of species, and to ensure a thin double layer for further reduction in EOF. The TE buffer consisting of 10 mM Tricine provides higher accumulation rates at the expense of lower buffering capacity. Lower concentration could not be used as the assay's repeatability and robustness is compromised. Hepes, Tricine, Bistris, and PVP were obtained from Sigma-Aldrich (St. Louis, MO). HCl was obtained from Merck (Darmstadt, Germany). All buffer solutions were made using deionized water (DI) from a Millipore Milli-Q system (Billerica, MA). We measured buffer conductivities using a conductivity meter (PC700, Eutech Instruments, The Netherlands)

The experiments in a glass channel were performed on a commercially available isotropically etched microchip (NS12A, PerkinElmer, Waltham, MA) having channel dimensions of 90 μm x 20 μm (width x depth). Our chip consisted of 4 reservoirs connected by channels; the West reservoir was connected to the longest channel (45.59 mm long) which intersected three shorter channels, termed North (15.1 mm long), South (3.92 mm long) and East (7.38 mm long). We first cleaned the channel by flowing 200 mM NaOH for 1 min, followed by 1 M HCl for another 1 min, and then rinsed the channel with DI for 1 min. In each experiment, we applied vacuum to the West reservoir to fill the North, East and South reservoirs with 20 μL of LE. Once the channel was filled, we rinsed the West reservoir with DI water, and filled it with 20 μL of TE-analyte mixture. We then placed the positive electrode to the East reservoir, and grounded the West reservoir. We applied a voltage of 400 V across the channel, and simultaneously record the resulting electric current. The focused sample was imaged at eight stations, located 4.7, 9.7, 14.7, 25.7, 30.7, 35.7, 40.7 and 44.7 mm from the TE reservoir. At each station, the images were background corrected (background was taken in the LE solution, before ITP plug arrives).

The process of running ITP on our fabricated μPAD is presented in Fig. 4. For convenience, we separated the process into two steps to allow filling of multiple channels simultaneously. We began by adding 150 μL of LE to the right reservoir, and relied on capillary action for filling the channel with LE solution (Fig. 4b,c). We allowed sufficient time (~10 min) for the liquid to reach a designed wax barrier, where it stopped (Fig. 4d). We then located the chip on the microscope, placed the electrodes in each of the reservoirs, and added another 150 μL of LE to the right reservoir. We then filled the left reservoir with 300 μL of a TE-analyte mixture (Fig. 4e,f). Importantly, the left-most part of the channel is initially exposed to air (i.e. is not covered by tape), and after adding the buffers serves as the initial contact point of the LE and TE. We applied 200 V across the channel to initiate ITP. Figures 4g and 4h respectively present the resulting focused ITP plug, as imaged by a consumer grade camera (SX510 HS, Canon, Tokyo, Japan) and by the microscope. The focused sample was imaged at eight stations, located at 0.75, 1, 1.25, 1.5, 1.75, 2, 2.25 and 2.5 cm from the TE reservoir (stations are printed as 1-8 on the paper-chip in

Fig. 4). At each station, the images were background corrected (background was taken in the LE solution, before ITP plug arrives).

To enable processing of large sample volumes, we designed our paper channel to be 2.5 mm wide. Under the applied voltage of 200 V, the electric currents established are on the order 100 to 1,000 μA. Large reservoir volumes are thus required for three primary reasons: (i) provide sufficient hydration for the paper, compensating any residual evaporation; (ii) Provide sufficient buffering from electrolysis[37]; and (iii) provide sufficient sample volume to be processed by the ITP channel. Our design supports 300 μL in each of the reservoirs, which, as further demonstrated in the experimental results section, provides sufficient sample to maintain a repeatable and stable process for over 10 min.
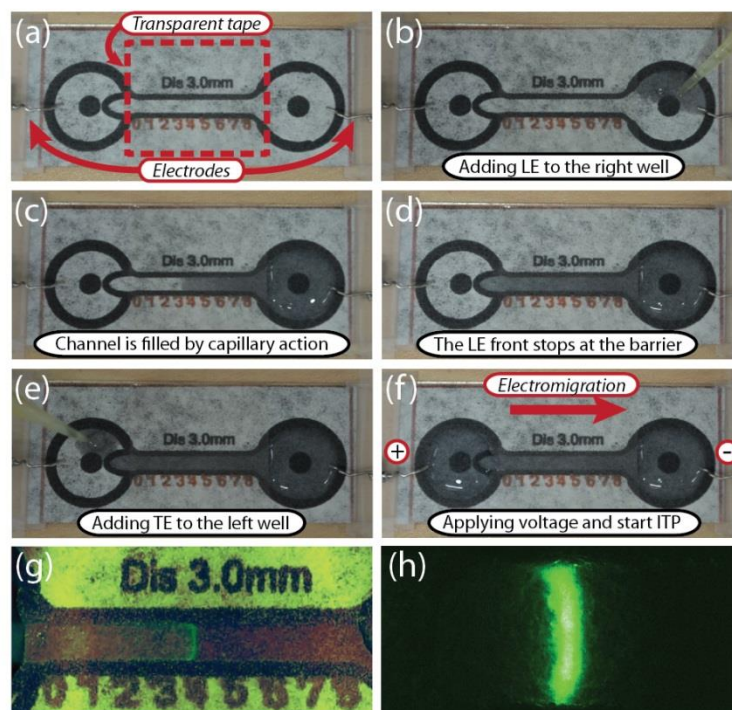
Figure 4. *Demonstration of the use of our fabricated μPAD for ITP focusing. (a) We place electrodes in each of the reservoirs. The area covered by masking tape is indicated by the dashed line. (b) We add the LE solution to the right reservoir. (c) The channel is filled with the LE buffer by capillary action (d) After ~10 min the LE front stops at the wax barrier (e) We add a TE-sample mixture to the left reservoir (f) Contact is formed between the TE and LE buffers, and ITP automatically initiates. (g) Raw fluorescence image of ITP focusing of 1μM fluorescein on a filter paper, imaged by a consumer-grade camera (h) Typical fluorescence image of ITP focusing imaged under a microscope. The device's length, end-to-end, is ~5 cm.*

11

4. Results and discussion

4.1. ITP focusing on µPAD

As illustrated qualitatively in Fig. 4g, at high initial concentrations ($> 1\mu M$) the ITP plug can be seen by naked eye or imaged by consumer-grade camera. However, the quantitative analysis presented in this and subsequent sections utilize significantly lower concentrations and has been performed based on microscopy imaging.

Fig. 5 presents quantitative experimental results of ITP focusing on our µPADs in a continuous injections scheme (i.e. sample mixed in the TE reservoir). Fig. 5c presents raw fluorescence images of the ITP front at the different stations along the paper channel. While the sample zone appears significantly more dispersed compared to sample focusing observed in standard glass microchannels, focusing is nevertheless clearly evident and the ITP plug is well contained and steadily electromigrates along the paper channel. Fig. 5a,b present respectively the width averaged concentration along the channel, during ITP, and the total sample accumulation. We convert each image from intensity values to concentrations through the calibration curve of each substrate (see Supplementary Information for complete details), and average those concentrations across the width of channel. We then calculate the total accumulated sample at each station by integrating all concentrations greater than 10% of the maximum, and multiplying by the width, depth, and porosity of the channel (for details regarding porosity measurements see Supplementary Information). Fig. 5b presents the total accumulated sample as a function of time with the solid line representing a fit to $N_a(t)$ expressed by eq.(13), with η serving as the free fitting parameter.
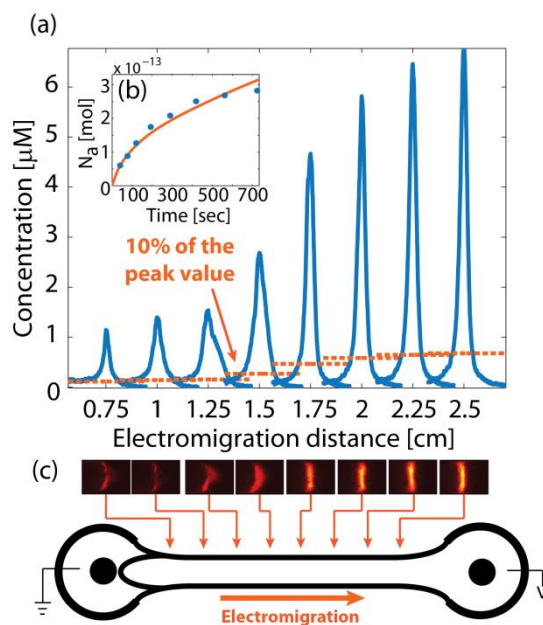
Figure 5. *Experimental results showing continuous ITP focusing of a fluorescent dye in a filter paper channel. We injected 10 nM DyLight650 into the TE, and measured fluorescence intensities during ITP, at fixed distances from the TE reservoir. (a) Width averaged concentration profiles registered at each station. (b) Total accumulated sample at each station (calculated using values above 10% of the peak value threshold), showing continuous accumulation of sample at the interface. The solid line represents a fit to $N_a(t)$ expressed by eq.(13). (c) Raw intensity images corresponding to each station. LE is 100 mM HCl and 200 mM BisTris; TE is 10 mM Tricine and 20 mM BisTris. For both buffers we used 1% of PVP.*

12

4.2. Characterization of ITP extraction efficiency on µPAD

The value of η, defined in eq.(13), describes the ratio between the number of sample molecules accumulated to the total amount of current passed in the system during ITP and the initial concentration of the analyte in the well. Since η depends only on the properties of the participating species (i.e. buffers and analyte), for a given system of chemistries, the value of η should be identical for glass and paper. However, discrepancy in measured values of η may occur as a result of the substrate itself (e.g. due to adsorption) or of the physical setup (e.g. pH changes in the reservoirs, or depletion of sample from the reservoir). Thus, η (units of $[lit\,A^{-1}sec^{-1}]$) can serve as an excellent indicator for the relative efficiency, or processing ability, of a specific substrate or setup.

Assuming a fully ionized analyte mobility of $36\times10^{-9}\,[m^2V^{-1}sec^{-1}]$ as estimated by Milanova *et al.*[38] we use Spresso[31] to compute the value of η for the TE chemistry consisting of 100 mM Hepes and 200 mM Bistris, and obtain a value of $1.3\times10^{-4}\,[lit\,A^{-1}sec^{-1}]$. Fig. 6a presents experimental results for this chemistry, showing the value of η as a function of time for both the glass channel and the paper channels. Importantly, both setups yield a near constant value at steady state, consistent with the analytical model. The mean value obtained in the glass channel is $1.3\times10^{-4}\,[lit\,A^{-1}sec^{-1}]$, which is identical to the numerical prediction. We thus consider the experiments in glass to be the accurate reference value. For the paper however, while theory predicts the same η value, in practice we obtained a measured value of $0.88\times10^{-5}\,[lit\,A^{-1}sec^{-1}]$ which is an order of magnitude lower than in glass.

Three main reasons could cause this behavior and reduce paper efficiency compared to glass: (i) adsorption of the analyte to the paper and/or wax (ii) decrease of analyte concentration in the TE reservoir, and (iii) decrease in the influx of sample ions into the channel, due to diffusion rate limitations. We will here address each of these possibilities: (i) We have ruled out adsorption by performing several ITP experiments in which we have injected a finite amount of sample to the paper channel and monitored the total amount of focused sample in time (see Supplementary Information for complete details). Results clearly showed no decrease in focused sample, indicating no adsorption of dye to the µPAD. (ii) Since in our design, the volume of the channels (in the order of several µL) is not negligible compared to the reservoir volume (in the order of hundreds of µL), dilution of sample in the reservoir could arise both from EOF delivering more liquid to the TE reservoir, and from rapid depletion of sample ions as they enter the channel. This change in concentration is expressed by eq.(14). From observing the electromigration velocity, we estimate the upper bound for EOF to be $u_{EOF} \sim 5\times10^{-4}\,[m\,sec^{-1}]$. Assuming a cross-section area of $8\times10^{-8}\,[m^2]$, and a total run time of ~700 sec, the total volume that enters the TE reservoir as a result of EOF during our typical experiment is ~30 µL. While this is a significant volume, it is still small compared to the $300\,\mu L$ volume of the reservoir. Thus we obtain $V_0 \gg \int_0^t u_{EOF} A_e dt$.

Furthermore, our experimental results show the accumulated sample, N_a, to be on the order of $3\times10^{-13}\,[mol]$, while the amount of sample in the reservoir, N_0, is $3\times10^{-12}\,[mol]$, and we may therefore assume $N_0 \gg \int_0^t \frac{dN_a}{dt}dt$. The average concentration in the reservoir can thus be approximated to be constant. (iii) The large size (width) of the channel may result in a situation where the diffusion rate of

13

new sample ions to the channel entrance is not sufficient to compensate for the high flux into the channel. Taking a characteristic length scale of $h = 1$ mm (corresponding both the characteristic diameter and height of the reservoir), one can define the characteristic electromigration time as $\tau_E = h / \mu_A E^{TE}$ and the characteristic diffusion time as $\tau_D = h^2 / D_A$. Estimating the diffusion coefficient from Einstein relation as $D \simeq 8.5 \times 10^{-10}\ [m^2\,sec^{-1}]$, and assuming an electric field of $E \sim 10^4\ [V\,m^{-1}]$, we obtain $\tau_E \sim 1\ [sec]$ vs. $\tau_D \sim 10^3\ [sec]$. This analysis neglects free convection which likely exists in the reservoir to some extent, but nevertheless shows a discrepancy in the time scales which may result in depletion of sample from the entrance to the channel. As we have ruled out other factors, we hypothesize that diffusion limits indeed play a dominant role in the efficiency of the assay. It is however important to note that while efficiency is lower, the absolute volume being processed by the paper channel is significantly larger than that of the glass microchannel due to its larger dimensions.
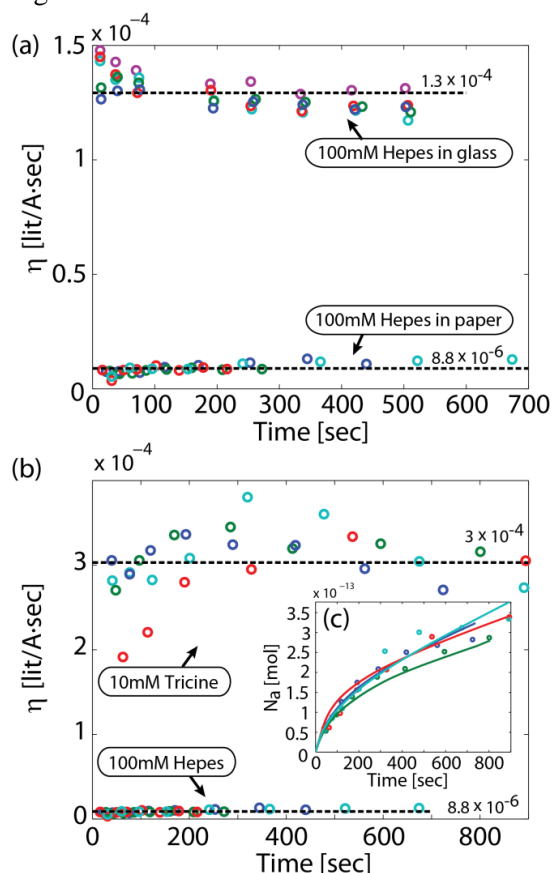
Figure 6. Experimental characterization of ITP focusing on paper (a) Experimental results for paper (five repeats) and glass (four repeats) showing the efficiency parameter η (ratio of total accumulated sample to the integral of current and initial sample concentration), registered at each station. The horizontal black dashed lines represent the mean value of η. The value obtained in paper is 8.8×10^{-6} [lit $A^{-1} sec^{-1}$], vs 1.3×10^{-4} [lit $A^{-1} sec^{-1}$] in glass, indicating only 7% efficiency of paper compared to glass. TE is 100 mM Hepes, 200 mM Bistris, and 1% PVP. (b) Experimental results (four repeats) showing that the reducing in mobility and total concentration of the TE (from 100 mM Hepes, 200 mM BisTris to 10 mM Tricine, 20 mM BisTris) results in a 34-fold improvement in the focusing rate. (c) The total accumulated sample in moles, as a function of time, registered at each station, obtained for the Tricine-based experiments. The trend lines represent a fit to $N_a(t)$, expressed by eq.(13), with η serving as the free fitting parameter.

4.3. Demonstration of 1,000-fold sample focusing

For a given analyte mobility, in order to maximize the amount of sample focused at the ITP interface, eq.(12) suggests minimizing the TE mobility, as well as reducing the TE concentration to allow a larger increase in analyte concentration across the TE adaptation region. We thus replace Hepes (pKa 7.5) by Tricine (pKa 8.15) resulting in an expected reduction in effective TE mobility from $8.1 \times 10^{-9}\,[m^2 V^{-1} sec^{-1}]$ to $5.6 \times 10^{-9}\,[m^2 V^{-1} sec^{-1}]$, and reduce the TE concentration from 100 mM to 10 mM. Fig. 6b presents the experimentally measured η for the two TE chemistries, showing a 34-fold improvement ($3 \times 10^{-4}\,[mol\,A^{-1} sec^{-1}]$ vs. $8.8 \times 10^{-6}\,[mol\,A^{-1} sec^{-1}]$) in sample accumulation with the 10 mM Tricine chemistry.

Fig. 6c presents the total accumulated sample (in moles) as registered at each station, using the 10 mM Tricine 20 mM Bistris TE chemistry. The total sample accumulated is approximately $3 \times 10^{-13}\,[mol]$, which was achieved after 700 sec. Since the initial concentration of the analyte in the TE reservoir is 10 nM, the total sample volume which was processed by ITP, evaluated by $\dfrac{N_a(t)}{c_0}$, is 30 μL.

We have thus far addressed the total amount of sample accumulated at the ITP interface. Fig. 7 provides a quantitative evaluation of peak (maximum) and average concentration of the focused sample. Peak value is important for detection and imaging applications where focusing is used to directly increase the signal to be detected (e.g. of a fluorescent molecule). However, in application where ITP is used to accelerate the reaction between co-focusing species, it is the average concentration which, to first order approximation, determines the rate of reaction.[39]

Fig. 7a presents a typical raw fluorescence image of the focused sample. At each station, to reduce noise associated with this measurement, we apply 5x5 binning to the ITP plug image and convert it to concentrations via the calibration curve (see Supplementary Information for complete details). We find the peak concentration by picking the highest value in the resulting image. Fig. 7b presents the width averaged concentration profile. We find the averaged concentration by averaging all concentrations greater than 10% of the maximum. Fig. 7c presents the peak and average focusing ratios as a function of time. Results show that over a 5 min duration, paper-based ITP provides average concentration enhancement of 200-fold, while the peak concentration is increased by 1,000-fold.
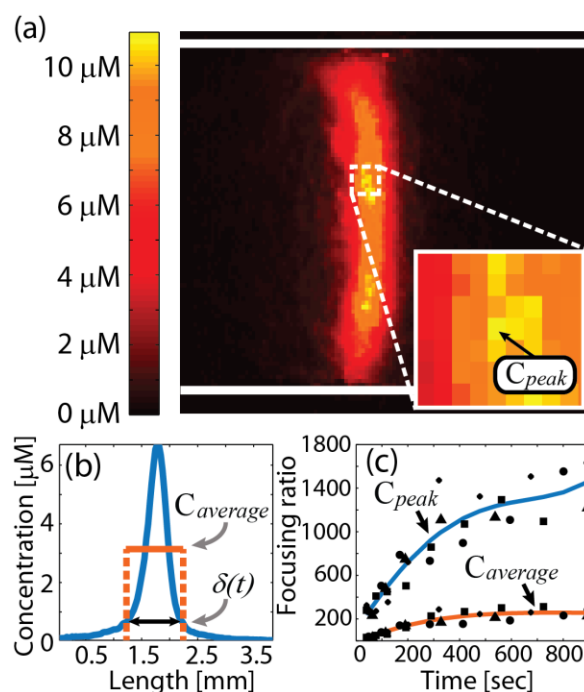
Figure 7. *Experimental measurements of focusing ratio achieved in paper ITP (a) Raw fluorescence image of the focusing zone. The analyte's maximum concentration is denoted by C_{peak}. (b) We calculate the width averaged concentration (blue line) of the analyte, and denote δ(t) as the full width of the profile at 10% of the maximum value. We denote the average concentration in that region as $C_{average}$. (c) Measurements of C_{peak}, and $C_{average}$, based on four repeats. Each marker shape represents an individual experiment, and 4th order polynomial fits, based on the average of all experiments, are presented solely to guide the eye. Results show that paper-based ITP provides average concentration enhancement of 200-fold, while the peak concentration is increased by 1,000-fold in less than 6 minutes.*

5. Conclusions

We presented an experimental and analytical study of a novel paper-based analytical device for sample focusing using isotachophoresis. We showed that although dispersion is much more significant in paper than in glass, substantial sample focusing (on the order of 1,000-fold) can be achieved in several minutes. Choosing or modifying the parameters of the porous media in order to minimize this dispersion remain an interesting and potentially important direction for research. Obtaining high sample concentrations in paper has direct implications in accelerating reaction kinetics[39] and creating low-cost devices with much enhanced sensitivity.

Another benefit of paper-based ITP is the ability to process large sample volumes. While microchannels are an excellent platform for ITP, their small dimensions typically limit their application to the analysis or processing of small sample volumes. Implementation of ITP in larger channels or larger diameter capillaries is challenging due to hydrodynamic instabilities and excessive joule heating. Paper (and porous media in general) offers the ability to reach large sample volumes while maintaining high hydrodynamic resistance in a planar format. In our work, we had used 2.5 mm wide channels and demonstrated processing of 30 μL of sample in several minutes. However, we see no fundamental reason why the width

16

of the channel could not be substantially increased to enable processing of hundreds of μL and even mL. This would open the door to the use of ITP for detection of extremely dilute samples (e.g. detection of bacteria at 10-100 copies per mL).

Managing joule heat and limiting evaporation are key challenges in integrating electrophoretic techniques with paper-based devices. While many other techniques for fabrication of paper-based devices exist, we find that wax printing is particularly suitable for obtaining shallow channels which result in higher surface to volume ratio of the channels and thus faster dissipation of the heat. Nevertheless, one could envision other methods for achieving this goal, with the most simple being the use of paper sheets of smaller initial thickness. However, to the best of our knowledge such substrates are currently not commercially available.

Our analytical model provides a convenient figure of merit for evaluating the efficiency of ITP focusing. Using this figure we showed that, despite the demonstrated gains, the efficiency of our device is roughly 10%, i.e. the amount of sample accumulated is only a fraction of the theoretical limit. By eliminating other potential reasons, we showed that this reduced efficiently is likely due to diffusion limits within the sample reservoir. Further investigation of these limitations is warranted, but it suggests that an order of magnitude improvement on all parameters is possible with further optimization.

We believe that the device and the analysis we had presented can serve to guide the design of low-cost, rapid and highly sensitive paper-based diagnostic platforms.

6. Acknowledgments

7. References

1. A. W. Martinez, S. T. Phillips, M. J. Butte, and G. M. Whitesides, *Angew. Chem. Int. Ed.*, 2007, **46**, 1318–1320.
2. A. K. Yetisen, M. S. Akram, and C. R. Lowe, *Lab. Chip*, 2013, **13**, 2210–2251.
3. A. W. Martinez, S. T. Phillips, G. M. Whitesides, and E. Carrilho, *Anal. Chem.*, 2010, **82**, 3–10.
4. E. Fu, P. Kauffman, B. Lutz, and P. Yager, *Sens. Actuators B Chem.*, 2010, **149**, 325–328.
5. E. Fu, T. Liang, J. Houghtaling, S. Ramachandran, S. A. Ramsey, B. Lutz, and P. Yager, *Anal. Chem.*, 2011, **83**, 7941–7946.
6. A. K. Ellerbee, S. T. Phillips, A. C. Siegel, K. A. Mirica, A. W. Martinez, P. Striehl, N. Jain, M. Prentiss, and G. M. Whitesides, *Anal. Chem.*, 2009, **81**, 8447–8452.
7. A. W. Martinez, S. T. Phillips, G. M. Whitesides, and E. Carrilho, *Anal. Chem.*, 2010, **82**, 3–10.
8. C.-M. Cheng, A. W. Martinez, J. Gong, C. R. Mace, S. T. Phillips, E. Carrilho, K. A. Mirica, and G. M. Whitesides, *Angew. Chem. Int. Ed.*, 2010, **49**, 4771–4774.
9. A. W. Martinez, *Bioanalysis*, 2011, **3**, 2589–2592.
10. F. Kohlrausch, *Ann. Phys.*, 1897, **298**, 209–239.
11. J. Kendall and E. D. Crittenden, *Proc. Natl. Acad. Sci. U. S. A.*, 1923, **9**, 75–78.
12. L. G. Longsworth, *J. Am. Chem. Soc.,* 1930*,* **52,** 1897–1910.
13. L. G. Longsworth, *Chem. Rev.*, 1942, **30**, 323–340.
14. H. G. Kunkel and A. Tiselius, *J. Gen. Physiol.*, 1951, **35**, 89–118.
15. O. Smithies, *Biochem. J.*, 1955, **61**, 629–641.
16. S. Hjertén, *Chromatogr. Rev.*, 1967, **9**, 122–219.

17. A. Vestermark and B. Sjödin, *J. Chromatogr. A*, 1972, **72**, 588–592.
18. V. Taglia and M. Lederer, *J. Chromatogr. A*, 1973, **77**, 467–471.
19. V. Taglia, *J. Chromatogr. A*, 1973, **79**, 380–382.
20. G. I. Abelev and E. R. Karamova, *Mol. Immunol.*, 1989, **26**, 41–47.
21. T. Toda, T. Fujita, and M. Ohashi, *Anal. Biochem.*, 1982, **119**, 167–176.
22. G. I. Abelev and E. R. Karamova, *Anal. Biochem.*, 1984, **142**, 437–444.
23. P. Mandal, R. Dey, and S. Chakraborty, *Lab. Chip*, 2012, **12**, 4026.
24. L. Ge, S. Wang, S. Ge, J. Yu, M. Yan, N. Li, and J. Huang, *Chem. Commun.*, 2014.
25. B. Y. Moghadam, K. T. Connelly, and J. D. Posner, *Anal. Chem.*, 2014, **86**, 5829–5837.
26. T. K. Khurana and J. G. Santiago, *Anal. Chem.*, 2008, **80**, 6300–6307.
27. S. Yao and J. G. Santiago, *J. Colloid Interface Sci.*, 2003, **268**, 133–142.
28. S. Zeng, C.-H. Chen, J. C. Mikkelsen Jr., and J. G. Santiago, *Sens. Actuators B Chem.*, 2001, **79**, 107–114.
29. M. Jaroš, K. Včeláková, I. Zusková, and B. Gaš, *ELECTROPHORESIS*, 2002, **23**, 2667–2677.
30. V. Hruška, M. Jaroš, and B. Gaš, *ELECTROPHORESIS*, 2006, **27**, 984–991.
31. M. Bercovici, S. K. Lele, and J. G. Santiago, *J. Chromatogr. A*, 2009, **1216**, 1008–1018.
32. F. P. Incropera, A. S. Lavine, and D. P. DeWitt, *Fundamentals of Heat and Mass Transfer*, John Wiley & Sons, 2011.
33. E. Carrilho, A. W. Martinez, and G. M. Whitesides, *Anal. Chem.*, 2009, **81**, 7091–7095.
34. Y. Lu, W. Shi, L. Jiang, J. Qin, and B. Lin, *ELECTROPHORESIS*, 2009, **30**, 1497–1500.
35. Y. Lu, W. Shi, J. Qin, and B. Lin, *Anal. Chem.*, 2010, **82**, 329–335.
36. R. Pelton, *TrAC Trends Anal. Chem.*, 2009, **28**, 925–942.
37. A. Persat, T. A. Zangle, J. Posner, J. G. Santiago, *Lab on a Chip* (Chips & Tips), 2007, 1–8.
38. D. Milanova, R. D. Chambers, S. S. Bahga, and J. G. Santiago, *ELECTROPHORESIS*, 2011, **32**, 3286–3294.
39. M. Karsenty, S. Rubin, and M. Bercovici, *Anal. Chem.*, 2014, **86**, 3028–3036.